AAS 12-208

SENSITIVITY ANALYSIS OF THE NON-GRAVITATIONAL PERTURBATIONS ON A MERCURY ORBITER

Takahiro Kato,[*] Benny Rievers,[†]
Jozef C. van der Ha[‡] and Claus Laemmerzahl[§]

This paper presents the effects of the non-gravitational forces acting on a Mercury orbiter. The Albedo and InfraRed radiations originating from Mercury's surface are expected to significantly influence the orbital motion of the orbiter. Therefore, we study the accelerations induced by the Albedo and InfraRed radiations from Mercury in addition to the Solar Radiation Pressure and the Thermal Recoil Pressure. In order to illustrate the practical relevance of the results, we employ the parameters and orbital elements of NASA's MESSENGER mission. The contributions of the Albedo reflection and the planetary InfraRed radiation have been formulated in terms of a straightforward practical model. The Thermal Recoil Pressure effects are within the range from 19 to 24 % relative to the SRP effects in the cases considered. They dominate the Albedo and InfraRed effects, at least in the direction along the Sun vector.

INTRODUCTION

Mercury is the least studied of the inner planets in the solar system. A substantially improved knowledge of the planet Mercury is required to improve our understanding of how the terrestrial planets formed and evolved. Therefore, the larger space agencies have or are planning exploration missions to Mercury, in particular NASA's MESSENGER and ESA/JAXA's Bepi Colombo.

Since Mercury is the closest planet to the Sun, a spacecraft orbiting around Mercury is exposed to severe solar fluxes almost 10 times higher than the flux at the distance of the Earth. Besides, the effects from the Albedo (ALB) and the InfraRed (IR) radiations originating from Mercury's surface are expected to have appreciable effects on the orbital motion of a Mercury orbiter. ALB refers to the sunlight reflected from the planet that acts on the satellite as a secondary light source in addition to the direct solar radiation. In a similar manner, we treat the planetary IR radiation as an additional radiation source. These radiations together with the incident solar flux induce Thermal Recoil Pressure (TRP) forces on the orbiter. TRP represents the reaction or recoil force induced by the heat emission from a spacecraft surface. Its magnitude depends on the surface temperature and emissive characteristics.

[*] Visiting Scientist, Center for Applied Space Technology and Microgravity, ZARM, University of Bremen, Am Fallturm, 28359 Bremen, Germany, takahiro117@gmail.com.
[†] Scientist, Department of Fundamental Physics, Center for Applied Space Technology and Microgravity, ZARM, University of Bremen, Am Fallturm, 28359 Bremen, Germany, benny.rievers@zarm.uni-bremen.de.
[‡] Consultant, Spacecraft Design and Operations, 5808 Bell Creek Rd, Deming, 98244 WA, USA, jvdha@aol.com.
[§] Professor, Department of Fundamental Physics, Center for Applied Space Technology and Microgravity, ZARM, University of Bremen, Am Fallturm, 28359 Bremen, Germany, claus.laemmerzahl@zarm.uni-bremen.de.

The non-gravitational perturbations of our interest are correlated as shown in Figure 1. Solar Radiation Pressure (SRP) is the most significant non-gravitational acceleration acting on a deep-space trajectory. However, the ALB and IR effects are not well known and are usually not incorporated in the orbit prediction and determination software. Furthermore, the absorbed planetary IR and ALB radiation energy may contribute to the TRP effect in addition to the direct solar radiation absorbed by the satellite's external surfaces.

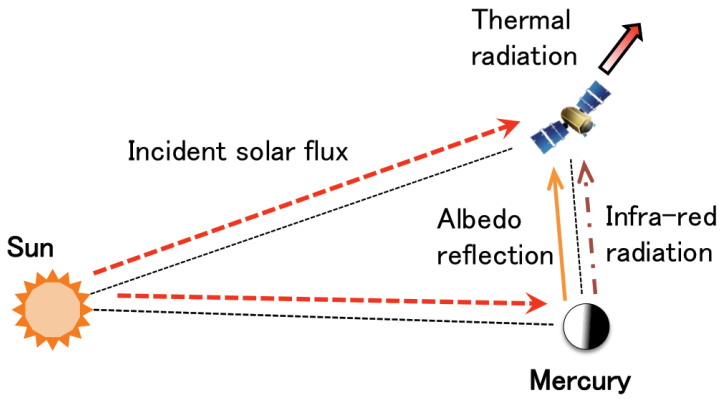

Figure 1. Overview of Radiation Effects Acting on a Mercury Orbiter.

Recently, a detailed study on the thermal accelerations acting on ESA's ROSETTA spacecraft was performed by the authors. [1, 2, 3, 4] The results show that the TRP acts predominantly in the same direction as the solar radiation force and has a magnitude of between 5 to 10 % of the SRP effects for Rosetta. Similar results have also been established for ESA's Mars Express and Venus Express satellites. [5]

Therefore, while taking account of the Mercury environment, we study here the effects of the ALB and the IR radiation from the planet Mercury in addition to those from the SRP and the TRP on the orbit of a Mercury orbiter. We perform specific simulation cases to investigate the individual contributions of the different perturbations, i.e. SRP, ALB, IR, and TRP. Since the gravity field of Mercury is not sufficiently well known, a Mercury orbiter will also be subjected to significant gravitational perturbations but we focus here only on perturbations induced by non-gravitational forces.

We take NASA's MESSENGER as a practical illustration and analyze the non-gravitational effects on its orbital elements. MESSENGER is successfully orbiting around the Mercury since March 18th, 2011 and preliminary operations results have already been published. [6, 7] In addition, the effects of ALB and IR on the MESSENGER spacecraft have been studied previously. [8] However, here we also include the TRP effects, which have not been considered yet and are expected to induce significant perturbations on an orbit in the Mercury environment.

NOTATIONS AND PERTURBATION MODELS

In the case of satellites in low orbits around the inner planets like Mercury and Venus, additional orbital perturbations will be generated by the thermal IR radiation emitted by the hot planetary surface. Furthermore, there may be appreciable contributions to the accelerations due to the ALB reflections from the planetary surface. The detailed study of these types of accelerations requires new approaches and different models compared to those that have been established for deep-space orbiters like Rosetta. [2, 3, 4]

Spacecraft Model and Notations

Figure 2 illustrates the spacecraft body and the reference frame of MESSENGER. Three ceramic-cloth sunshields protect the spacecraft against the intense solar radiation in Mercury orbit. Thus, the center sunshield is essentially (i.e., within about 12 degrees) kept normal to the Sun after the insertion into the Mercury orbit. The solar panels are specially designed and consist of two-thirds mirrors and one-third solar cells for thermal management.

The normal vector of each surface element is expressed in terms of the rotation angles *Right Ascension (RA)*, positive about the Z axis of the body frame (*RA* = 0 at X axis), and *Declination (DE)*, positive about the new (rotated) Y axis of the body frame.

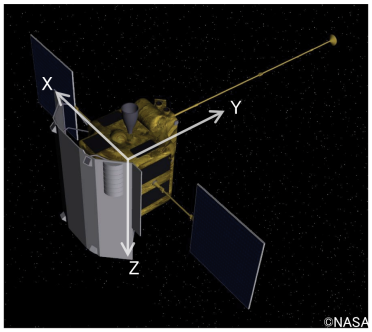

Figure 2. MESSENGER and Its Body Reference Frame.

We use a spacecraft configuration model containing the essential spacecraft external surfaces that are summarized in Table 1.[7] The back side of the spacecraft is also considered in addition to the main additional structural elements (i.e., Sun shields and the solar panel front/back sides). This is based on the expectation that the planetary ALB reflection and IR radiation irradiate these surface elements during parts of the spacecraft orbit around Mercury.

Table 1. Spacecraft Model Inputs.[7]

ID	Surface element	Area (A_k) [m^2]	*RA* [deg]	*DE* [deg]
1	-X sunshield wing	2.122	-127.2	0
2	Center sunshield	1.264	-90	0
3	+X sunshield wing	2.122	-52.8	0
4	+X facing (body)	2.350	0	0
5	+Z facing (body)	1.803	0	90
6	+Y facing (body)	4.612	90	0
7	+X solar panel, front	2.724	-90	0
8	-X solar panel, front	2.724	-90	0
9	+X solar panel, back	2.724	90	0
10	-X solar panel, back	2.724	90	0
11	-X facing (body)	2.350	180	0
12	-Z facing (body)	1.803	0	-90

In addition to these parameters, we need the surface thermo-optical parameters, in particular the absorptivity and specular/diffuse reflection coefficients. Due to the lack of information, we adopt preliminary estimates based on previous studies as baseline inputs.[1, 2]

Furthermore, we use a uniform emissivity parameter ε_{SC} (= 0.8) for all surface elements of the orbiter, except for the back sides of the solar panels. The emissivity of the back side of the solar panel is given by the following equation, which is valid for the Rosetta solar arrays. [1, 9]

$$\varepsilon_b = 0.312 + 3.29 \times 10^{-3} T_b - 5.33 \times 10^{-6} T_b^2 \tag{1}$$

Planet and Orbit Reference Frame

We introduce the Mercury-Sun fixed coordinate frame to express the orbit of the orbiter relative to Mercury, see Figure 3. The frame consists of the P_M axis pointing towards the Sun, the W_M axis normal to the orbit plane of Mercury, and the Q_M axis completes the right-hand coordinate system.

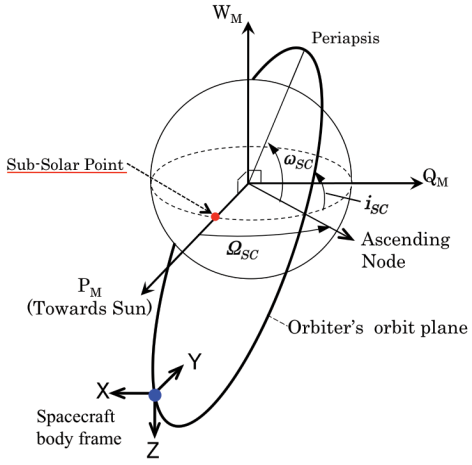

Figure 3. Mercury Reference Frame and Satellite Body Frame Relative to Mercury.

Here, we neglect the heliocentric progression of Mercury during one orbit period (i.e., 12 hours) of the orbiter. This means that one full orbiter revolution is propagated for each of the specified Mercury positions. The position of the orbiter in its orbit around Mercury is defined as $\mathbf{R}_{M\text{-}SC}$ in the Mercury's coordinate frame shown in Figure 3. It can be expressed as a function of true anomaly ν_{SC} by using the orbital elements of the orbiter as,

$$\mathbf{R}_{M \to SC} = \frac{a_{SC}(1 - e_{SC}^2)}{1 + e_{SC} \cos \nu_{SC}} \begin{bmatrix} \cos u_{SC} \cos \Omega_{SC} - \sin u_{SC} \cos i_{SC} \sin \Omega_{SC} \\ \cos u_{SC} \sin \Omega_{SC} + \sin u_{SC} \cos i_{SC} \cos \Omega_{SC} \\ \sin u_{SC} \sin i_{SC} \end{bmatrix} \tag{2}$$

where, u_{SC} ($u_{SC} = \omega_{SC} + \nu_{SC}$) is the argument of latitude.

Table 2 summarizes the achieved MESSENGER orbital elements.[6] We select several values for the right ascension of ascending node Ω_{SC} in addition to the orbital elements of MESSENGER to analyze the non-gravitational perturbation effects on the orbiter. By using the coordinate system in Figure 3, the unit Sun vector $\hat{\mathbf{s}}_M$ can be expressed as $\hat{\mathbf{s}}_M = [1\ 0\ 0]^T$.

Table 2. MESSENGER Achieved Orbital Elements in Mercury Orbit.

Semi-major axis	Eccentricity	Inclination i_{SC}	Argument of periapsis ω_{SC}
10175.39 [km]	0.740	82.52 [deg]	119.16 [deg]

We assume that the orbiter will always maintain the fixed Sun-pointing attitude, which implies that the –Y axis is always directed along P_M. In addition, we also assume that the XY plane of the spacecraft body frame remains parallel to the P_MQ_M plane of the Mercury coordinate frame, see Figure 3. Thus, we obtain the rotation matrix $\mathbf{R}^{MSC}$ from the orbiter body frame to the Mercury frame by using the 3-1-3 Euler angle rotations. Besides, we also find the rotation matrix $\mathbf{R}^{SCM}$ from planet frame to spacecraft body frame.

$$\mathbf{R}^{MSC} = \begin{bmatrix} 0 & -1 & 0 \\ -1 & 0 & 0 \\ 0 & 0 & -1 \end{bmatrix}, \quad \mathbf{R}^{SCM} = \left[\mathbf{R}^{MSC}\right]^{-1} = \begin{bmatrix} 0 & -1 & 0 \\ -1 & 0 & 0 \\ 0 & 0 & -1 \end{bmatrix} \tag{3a, b}$$

Planet Surface Model and View Factor

We need a planet surface model with corresponding view factors for the calculations of ALB and IR radiation effects. Therefore, we introduce a grid model on the planet surface with cells of uniform surface absorptivity and emissivity. From the geometrical relationships between the grid points on Mercury and the orbiter, the ratio of the emitted energy from each grid point on Mercury to a surface element of the orbiter can be obtained. This is done by a view factor in terms of the angles between the two unit vectors (i.e., normal to the surface element and normal to the grid point surface) and the line connecting the two surfaces.

Figure 4 shows the grid model introduced on the planet surface and Table 3 summarizes the parameters of Mercury model. [10,11] For the sake of simplicity, the relative distance of the Sun and Mercury d is obtained from the two-body equation and it will affect all the calculations including SRP and TRP. Thus, the incident solar flux S at distance d is obtained as $S(d) = S_0 / d^2$ [W/m^2], where S_0 is the solar flux at 1 AU (= 1366.1 [W/m^2]) and the relative distance d is expressed in AU. The resulting $S(d)$ is used as the incident solar flux received by Mercury's surface and also by the orbiter. We note that S varies with d, between 6272 [W/m^2]at aphelion and 14446 [W/m^2] at perihelion. For convenience, we simply use S from here on.

Table 3. Mercury Model Inputs.

Parameter	Symbol	Value
Semi-major axis [km]	a_M	57910000
Eccentricity	e_M	0.2056
Planet radius [km]	R_M	2440
Bond albedo coefficient	γ_M	0.12
Surface absorptivity	α_M	0.88
Surface emissivity	ε_M	0.82[12]
Number of grid in Azimuth direction	az	100
Number of grid in Elevation direction	el	50

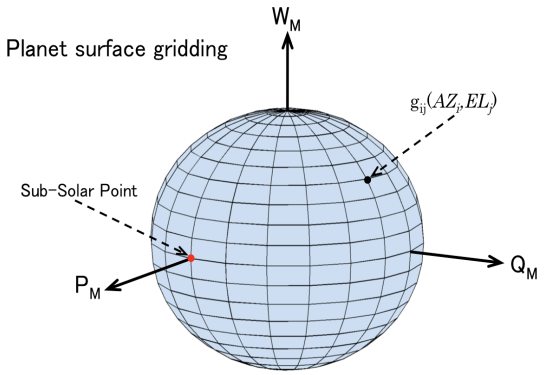

Figure 4. Grid Model on Mercury Surface.

The azimuth and elevation angles of a grid point g_{ij} are defined as,

$$AZ_i = -\pi + \frac{2\pi}{az}(i-1) \quad (for\ i = 1,2,...,az) \tag{4}$$

$$EL_j = -\frac{\pi}{2} + \frac{\pi}{el}(j-0.5) \quad (for\ i = 1,2,...,el) \tag{5}$$

Here, *az* and *el* are arbitrary positive integers that define the number of grid points in the azimuth and elevation directions, respectively, and *el* is defined as half of *az*. To avoid the concentration of grid points at both poles of the planet, we offset the grid points by half a grid from both planet poles.

Therefore, the position vector $\mathbf{R}_{ij}$ of each grid point in Mercury's frame and the unit normal vector $\mathbf{n}_{ij}$ at each grid point can be written as,

$$\mathbf{R}_{ij} = R_M \begin{bmatrix} \cos EL_j \cos AZ_i \\ \cos EL_j \sin AZ_i \\ \sin EL_j \end{bmatrix} = R_M \mathbf{n}_{ij} \tag{6}$$

where, R_M denotes the spherical radius of Mercury.

Eq. (6) together with the satellite position vector in Eq. (2) allow the computation of the fraction of the energy flux emitted by a Mercury grid point and received by a satellite surface element *k* by using the geometrical relationship shown in Figure 5. $\mathbf{R}_{g\text{-}SC,ij}$ and $\mathbf{R}_{SC\text{-}g,\ ij,\ k}$ are the line-of-sight vectors between the grid point g_{ij} and the orbiter surface element *k*, and $\mathbf{n}_k$ is the unit normal vector of surface element *k*.

However, for simplicity, we use the distance of each grid to the center of mass of the orbiter for all surface elements of the orbiter. This simplification does not affect the resulting accuracy as a few meter difference relative to hundreds or thousands of kilo meters has no appreciable influence. Hence, we can simplify the expression of the line-of-sight vector $\mathbf{R}_{SC\text{-}g,\ ij,\ k}$ from spacecraft to grid point on Mercury as $\mathbf{R}_{SC\text{-}g,\ ij}$.

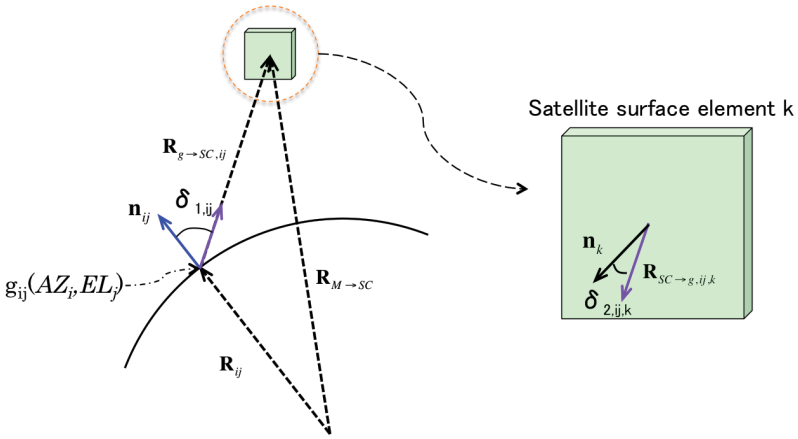

Figure 5. Geometry of Planet, Grid, and Surface Element of the Orbiter.

From these geometrical relationships shown in Figure 5, the ratio of the energy received by surface element k of the orbiter compared to the energy that is radiated by the planet grid point g_{ij} can be obtained by using the angles between the respective unit vectors, i.e. $\delta_{1,ij}$ and $\delta_{2,ij,k}$ in Figure 5. In addition, we assume that both radiations of ALB and IR represent hemispherically diffuse emissions.

Thus, we can compute the view factor $f_{ij,k}$ at each grid by using the area A_k and the surface normal $\mathbf{n}_k$ of the surface element k of the orbiter and the relative distance r_{ij} from each grid point to the orbiter center of mass as,

$$f_{ij,k} = \frac{\cos\delta_{1,ij}\cos\delta_{2,ij,k}}{\pi r_{ij}^2} A_k \tag{7}$$

The factor π has the unit of steradians [sr] and it is due to the geometrical integration process of the view factor and r_{ij} is equal to the length of the vector $\mathbf{R}_{g\to SC,ij}$ shown in Figure 5.[13] Thus, the view factor given in Eq. (7) is a non-dimensional coefficient for each of the grid points of the planet surface.

Furthermore, for each of the grid points on the planet surface, 0 is assigned for the view factor if one of the angles of $\delta_{1,ij}$ or $\delta_{2,ij,k}$ in Eq. (7) exceeds $\pi/2$.

Solar Radiation Pressure (SRP)

A spacecraft that is exposed to sunlight experiences accelerations induced by the absorption and reflection of photons on the exposed spacecraft surfaces. This phenomenon is known as Solar Radiation Pressure (SRP). SRP is typically the most significant non-gravitational acceleration acting on a deep-space trajectory. The origins and effects of the SRP are fairly well known and are incorporated in most existing orbit determination software.

The SRP acceleration model implemented for each surface element is expressed by using the unit Sun vector $\mathbf{s}$, unit normal vector $\mathbf{n}_k$, and optical parameters,

$$\boldsymbol{a}_{SRP,k} = -C_{SRP,k}\cos\theta_k\left\{\left(\alpha_k + \gamma_{d,k}\right)\mathbf{s} + 2\left[\frac{\gamma_{d,k}}{3} + \gamma_{s,k}\cos\theta_k\right]\mathbf{n}_k\right\} \tag{8}$$

with,

$$C_{SRP,k} = \frac{S}{c}\frac{A_k}{m_{SC}} \quad [m/s^2] \tag{9}$$

where, θ_k is the angle between the incident solar flux and the surface normal on the surface element k, S is the solar flux at heliocentric distance d, and m_{SC} is the mass of the orbiter. The subscript k refers to the ID of each surface element of the orbiter (as defined in Table 1). For a surface element k with $\theta_k \geq \pi/2$ we assign 0 for the SRP acceleration vector. In order to obtain the acceleration components in the spacecraft body frame, the vectors in Eq. (8) must also be expressed in the same frame.

Eclipses. In addition, we introduce the cylindrical shadow model as shown in Figure 6 to implement eclipses by Mercury. When using the coordinate frame introduced in Figure 3, cylindrical eclipses by Mercury can be determined from the geometry in Figure 6.

Since the P_M axis of the Mercury reference frame is always pointing to the Sun, the orbiter is illuminated by sunlight when the x component of the position vector obtained from Eq. (2) in the planet frame is positive, i.e. case A in Figure 6. When the x component of the position vector is negative, we need to distinguish two different cases: case B when the distance d_{yz} of the spacecraft relative to the P_M axis is larger than the radius of Mercury R_M, and case C when d_{yz} is smaller than R_M. It is clear from Figure 6 that case B is illuminated and that case C is in eclipse. We compute the eclipse condition of the orbiter at each point in its orbit around Mercury and assign 0 for the SRP acceleration vector if it applies.

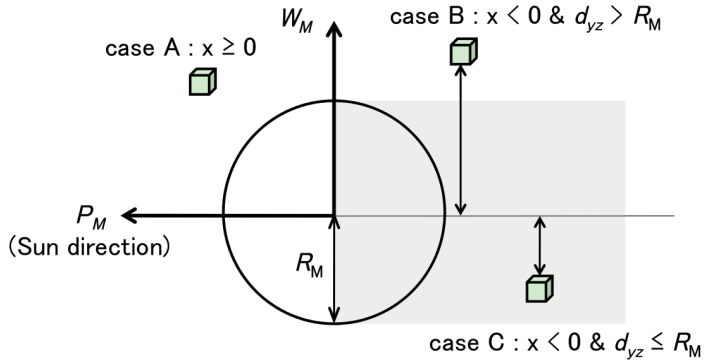

Figure 6. Cylindrical Mercury Eclipse Criteria.

Albedo (ALB) Reflection

The Albedo (ALB) effects are usually not incorporated in the orbit determination software. This is because the effects of ALB in low Earth orbit are usually negligible. However, the incident solar flux at Mercury's perihelion is almost 10 times higher than that at Earth distance. Therefore, it is of interest to investigate the ALB effects for the Mercury orbiter.

For the ALB model, we calculate the ALB energy reflected from each grid point by using the planar surface unit vector $\mathbf{n}_{ij}$, the incident Sun vector $\hat{\mathbf{s}}_M$ (in Mercury frame), and the area A_{ij} of the planet surface element,

$$ALB_{ij} = \gamma_M S(\mathbf{n}_{ij} \cdot \hat{\mathbf{s}}_M) A_{ij} \quad [W] \tag{10}$$

where, γ_M (= 0.12) is the bond albedo coefficient of Mercury and the surface area A_{ij} is obtained as follows,

$$A_{ij} = \frac{4\pi R_M^2 \cos EL_j}{az \times el} \quad [m^2] \tag{11}$$

When taking account of the view factor, we can express the energy received by the surface element k of the orbiter as,

$$Q_{ALB,ij,k} = f_{ij,k} ALB_{ij} \quad [W] \tag{12}$$

By using Eq. (12), we obtain the following equation to calculate the acceleration induced by the total planetary ALB radiation on each surface element of the orbiter,

$$\boldsymbol{a}_{ALB,k} = -\sum_i \sum_j C_{ALB,ij,k} \cos\delta_{2,ij,k} \left\{ \left(\alpha_k + \gamma_{d,k}\right) \mathbf{R}_{SC \to g,ij} + 2\left[\frac{\gamma_{d,k}}{3} + \gamma_{s,k} \cos\delta_{2,ij,k} \right] \mathbf{n}_k \right\} \tag{13}$$

where, $C_{ALB,\,ij,\,k}$ is the ALB acceleration coefficient similar to the SRP coefficient introduced in Eq. (9),

$$C_{ALB,ij,k} = \frac{Q_{ALB,ij,k}}{m_{SC} c} \quad [m/s^2] \tag{14}$$

Infrared Radiation (IR)

The InfraRed (IR) radiation originates from the heat flux emitted by the warm planetary surface under the influence of solar heating. Its effects are not at all well known and are usually not incorporated in the orbit determination software.

For the sake of simplicity, we use the homogeneous hemispherical temperature $T_{M,\,hemi}$ on the dayside Mercury surface, which can be expressed by using the steady state heat balance on Mercury's dayside hemisphere,

$$T_{M,hemi} = \left\{ \frac{\alpha_M S}{2\sigma\varepsilon_M} \right\}^{0.25} \quad [K] \tag{15}$$

here, α_M is the absorptivity and ε_M is the emissivity of Mercury's surface, respectively, and σ is the Stefan-Boltzmann constant. The resulting temperature on Mercury's illuminated hemisphere surface varies with the solar distance d: 608 [K] at perihelion and 493 [K] at aphelion.

By using $T_{M,\,hemi}$ in Eq. (15), we obtain a homogeneous IR energy radiated from each grid point as,

$$IR_{day,ij} = \varepsilon_M \sigma T_{M,hemi}^4 A_{ij} \quad [W] \tag{16}$$

Since we assume homogeneous temperature and emissivity, we have the same energy radiated from all the grid points on the day side of Mercury. At the same time, we assume homogeneous temperatures T_{night} (= 100 [K]) on the night side grids, so we also have,

$$IR_{night,ij} = \varepsilon_M \sigma T_{night}^4 A_{ij} \quad [W] \tag{17}$$

when taking account of the view factor, we can express the energy of the IR radiation that is received by the surface element k of the orbiter as,

$$Q_{IR,ij,k} = \begin{cases} f_{ij,k} IR_{day,ij} & (for\ day\ side) \\ f_{ij,k} IR_{night,ij} & (for\ night\ side) \end{cases} \quad [W] \tag{18}$$

Finally, in the same manner as done for the ALB, we obtain the following equation for the acceleration calculation.

$$\boldsymbol{a}_{IR,k} = -\sum_i \sum_j C_{IR,ij,k} \cos\delta_{2,ij,k} \left\{ \left(\alpha_k + \gamma_{d,k}\right) \mathbf{R}_{SC \to g,ij} + 2\left[\frac{\gamma_{d,k}}{3} + \gamma_{s,k} \cos\delta_{2,ij,k} \right] \mathbf{n}_k \right\} \tag{19}$$

with,

$$C_{IR,ij,k} = \frac{Q_{IR,ij,k}}{m_{SC} c} \quad [m/s^2] \tag{20}$$

Thermal Recoil Pressure (TRP)

The Thermal Recoil Pressure (TRP) is mainly induced by the re-emission of the incident solar radiation that has been absorbed by the satellite's external surfaces. In the case of planetary orbiters, the IR radiation and ALB fluxes may also introduce significant fluxes on the satellite surfaces in addition to the incident solar flux. Thus, we compute the temperatures of the spacecraft body surfaces by incorporating the resulting heat inputs from all of these radiation sources.

Figure 7 illustrates the heat inputs and outputs on the solar panel front and back sides. The heat inputs due to the ALB and IR depend on the orbital position and the attitude orientation of the orbiter relative to the planet. Here, we assume the nominal orientation of the solar panel that the front side is perpendicular to the incident solar radiation.

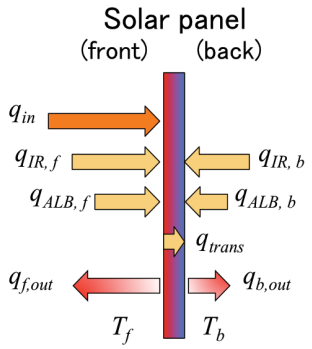

Figure 7. Heat Inputs and Outputs on Solar Panel Front/Back.

Here, q_{in} denotes the absorbed portion of the incident solar flux which is expressed by using the absorptivity α_f of the front side of the solar panel as $q_{in} = \alpha_f S$. When there is a temperature difference between the front side temperature T_f and the back side temperature T_b, the heat transfer inside the solar panel q_{trans} has to be taken into account.

Thus, we have the following heat balance equations,

$$q_{f,out} = \varepsilon_f \sigma T_f^4; \quad q_{b,out} = \varepsilon_b \sigma T_b^4 \tag{21}$$

$$q_{f,out} = q_{in} + q_{ALB,f} + q_{IR,f} - q_{trans} \tag{22}$$

$$q_{b,out} = q_{ALB,b} + q_{IR,b} + q_{trans} \tag{23}$$

The transferred heat flux q_{trans} from the warmer front side to the colder back side through the panel can be obtained by using the procedure established in the Rosetta study, [1,2] which is,

$$q_{trans} = k(T)\frac{0.95A_{Al}}{h}(T_f - T_b) + \sigma\frac{\varepsilon_i(1 - A_{Al})}{2 - \varepsilon_i}(T_f^4 - T_b^4) \tag{24}$$

It expresses the heat transfer through the solar panel in terms of a conducted part and a radiated part. We need the following parameters for the calculation: the conductivity $k(T)$, the thickness of solar panel h, the net aluminum cross-section per square meter of solar panel A_{Al}, and the inner core surface emissivity ε_i. However, due to the lack of specific information, we adopt the expression of Rosetta in Eq. (24) also for this study.

We assume that the total absorbed energy from three radiation sources described above is completely re-emitted from each surface element. By calculating the total heat inputs for each surface element by means of the respective view factors, we obtain the surface temperatures from the following equation.

$$T_k = \left(\frac{\alpha_k q_{tot,k}}{\varepsilon_{SC}\sigma}\right)^{0.25} \tag{25}$$

here, α_k is the absorptivity and $q_{tot,k}$ ([W/m^2]) is the total heat flux input from the incident Sun, ALB, IR of the surface element k, respectively.

Finally, by using the resulting temperature from Eq. (25), we can calculate the TRP acceleration acting on the surface element k as,

$$\boldsymbol{a}_{TRP,k} = -\frac{2}{3}\frac{\varepsilon_k \sigma T_k^4}{c}\frac{A_k}{m_{SC}}\mathbf{n}_k \tag{26}$$

SIMULATION METHODS AND CONDITIONS

For the sake of simplicity and practicality, we introduce several assumptions. Analytical solutions can be obtained by selecting the proper geometry of the Sun, Mercury, and spacecraft. Specific details of the assumptions and models are listed below. These are the bases of the presented analytical model and solutions.

- ✓ Mercury follows the two-body Kepler orbit about the Sun with zero inclination
- ✓ Mercury is a perfect sphere with uniform optical properties
- ✓ Surface temperatures of Mercury and the orbiter are at equilibrium state
- ✓ The orbiter maintains the (initial) MESSENGER orbit around Mercury
- ✓ The orbiter keeps its center sunshield always perpendicular to the Sun direction
- ✓ We neglect heat flow inside Mercury's core and the daily rotation of Mercury

Simulation Conditions

We define the following Mercury geometrical configurations as test cases to investigate the effects of non-gravitational perturbations on a Mercury orbiter, see Figure 8 and Table 4.

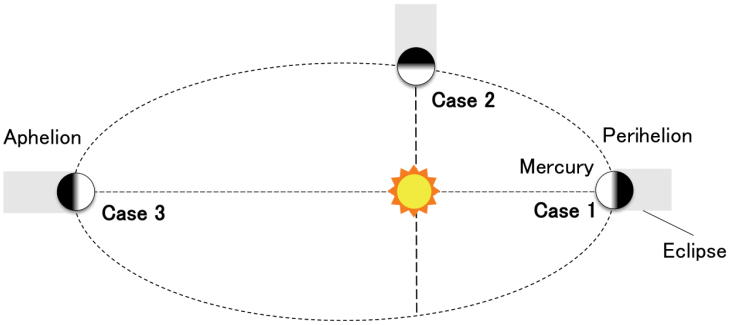

Figure 8. Selected Mercury Positions for Simulations.

Table 4. Simulation Inputs.

	Mercury true anomaly [deg]	Solar distance [km]
Case 1	0	4.60×10^7
Case 2	90	5.55×10^7
Case 3	180	6.98×10^7

For each of the three Mercury positions, 4 different orbit planes are defined for the orbiter as test cases as illustrated in Figure 9. By using the planet reference frame in Figure 3, each of the test case orbits around Mercury is expressed by the Local Time of Ascending Node (LTAN) as shown in Figure 9. The Noon (LTAN 12 am) orbit passes over the sub-solar point and has an eclipse interval. On the other hand, the 6 pm orbit is always illuminated by the incident Sun.

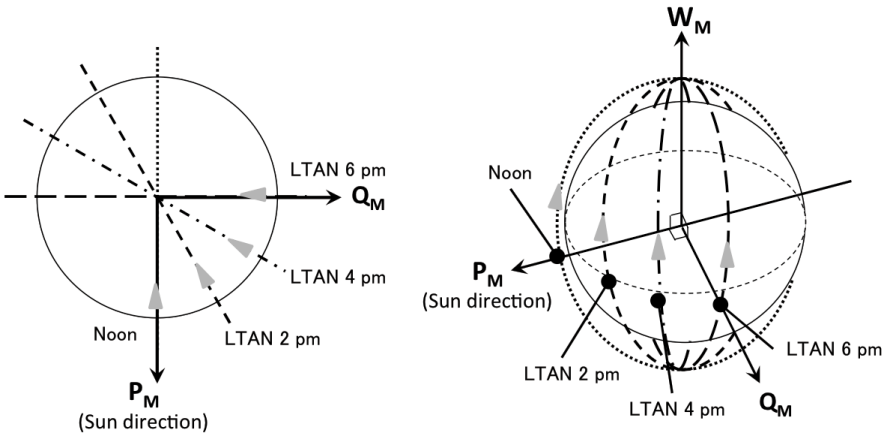

Figure 9. Local Time of Ascending Node Variations.
Left : Polar View of Node Lines, Right : 3D View.

RESULTS AND DISCUSSIONS

For all cases described above, we compute the accelerations acting on the orbiter induced by the SRP, ALB, IR, and TRP effects. We analyze the variations of these effects with respect to the orbital LTAN values and the different Mercury positions.

We present in Figure 10 the total magnitude and the individual contributions of each of the perturbations along X, Y, Z axes of the spacecraft body frame for Case 1 and a Noon orbit. The horizontal axes represent the true anomaly of the orbiter (true anomaly = 0 at periapsis, see Figure 3). The contributions and directions of each individual perturbation are explicitly shown in the last 3 plots in Figure 10.

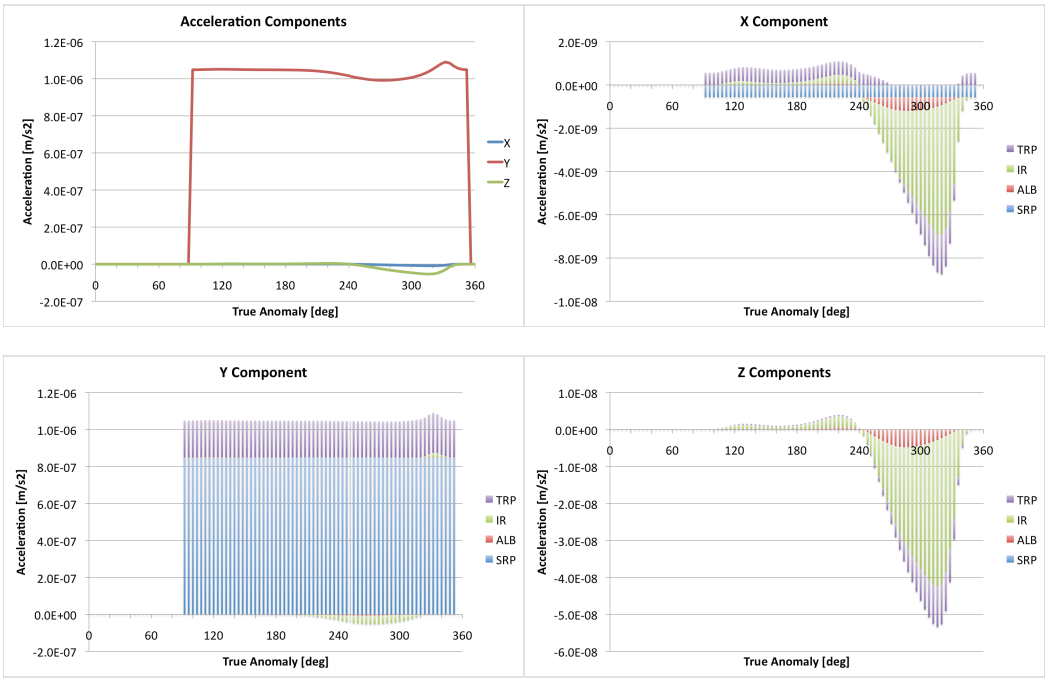

Figure 10. Resulting Acceleration Components over One Revolution in Case 1, Noon Orbit. Top Left : Total magnitude, Top Right : X, Bottom Left : Y, Bottom Right : Z Components.

It is clear that the IR effect is dominant in the X and Z directions for the case shown in Figure 10. However, the major perturbations are still due to the SRP and TRP effects along the Sun direction (Y direction) and TRP has about 24% of the SRP magnitude. As expected, the TRP has significant effect in the Mercury environment.

We find that peaks of the X and Z components appear after the true anomaly of 240°. This value corresponds with the position of the sub-solar point and, at the same time, is the ascending node (See Figure 3). After the true anomaly has passed 240°, the orbiter approaches towards the periapsis. Thus, the relative distance of the orbiter and Mercury surface become closer and the effects from the ALB and IR increase as shown in Figure 10.

LTAN Effects

First, we analyze the variations induced by different values of LTAN under a fixed Mercury position. Figure 11 shows the magnitudes of the resulting accelerations from each perturbation source of ALB, IR, and TRP for 4 different LTAN orbits, and Mercury at its perihelion (Case 1). The horizontal axis is the true anomaly of the orbiter. In the analytical model the magnitude of the SRP acceleration is constant at 8.49×10^{-7} m/s^2 in Case 1 for all LTAN values.

We found that the contribution of the TRP effect with respect to the SRP acceleration is in general close to constant at about 24 % for all cases. In addition, except for the 6 pm orbit, there are eclipses by Mercury where all the non-gravitational perturbations essentially vanish.

The fluctuations in the IR and ALB are induced by the number of visible girds on Mercury seen by the orbiter and by the relative distance of the orbiter and Mercury's surface. The number of visible grids is proportional to the view factor (i.e., energy flux received by the orbiter). On the other hand, the relative distance affects the radiated power by its inverse square law.

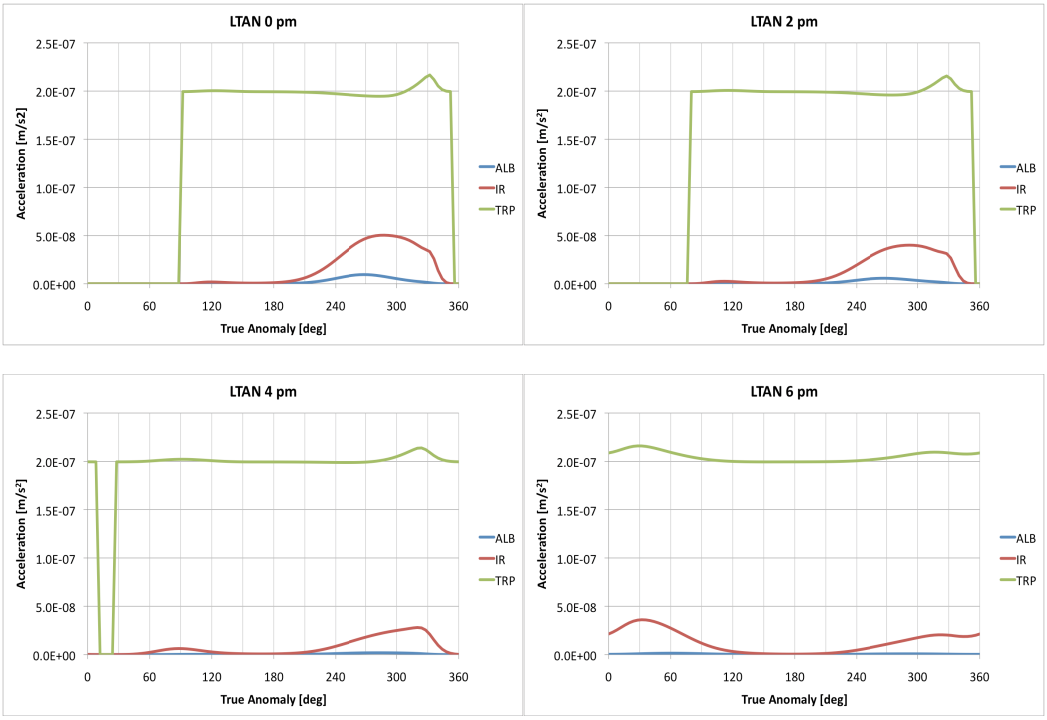

Figure 11. Resulting Acceleration Magnitudes for Different LTAN Values.
Top Left : Noon, Top Right : 2 pm, Bottom Left : 4 pm, Bottom Right : 6 pm.

It is interesting that the IR effects have its peak in the Noon orbit at true anomaly of about 300, not at 240 (which would be above the sub-solar point, see Figure 3). This is due to the view factor fluctuations as mentioned above.

In addition, the ALB and IR effects reduce with an increase in LTAN (Ω_{SC}). This is because the ascending node of the orbiter moves away from the sub-solar point for an increasing LTAN value.

Mercury Position Effects

The ratios of the smaller (i.e., ALB, IR, TRP) accelerations relative to the SRP effects for each Mercury position are shown in Figure 12 as a function of the orbiter's true anomaly. Table 5 provides the SRP acceleration magnitudes and average contributions of non-gravitational perturbations relative to the SRP for each case.

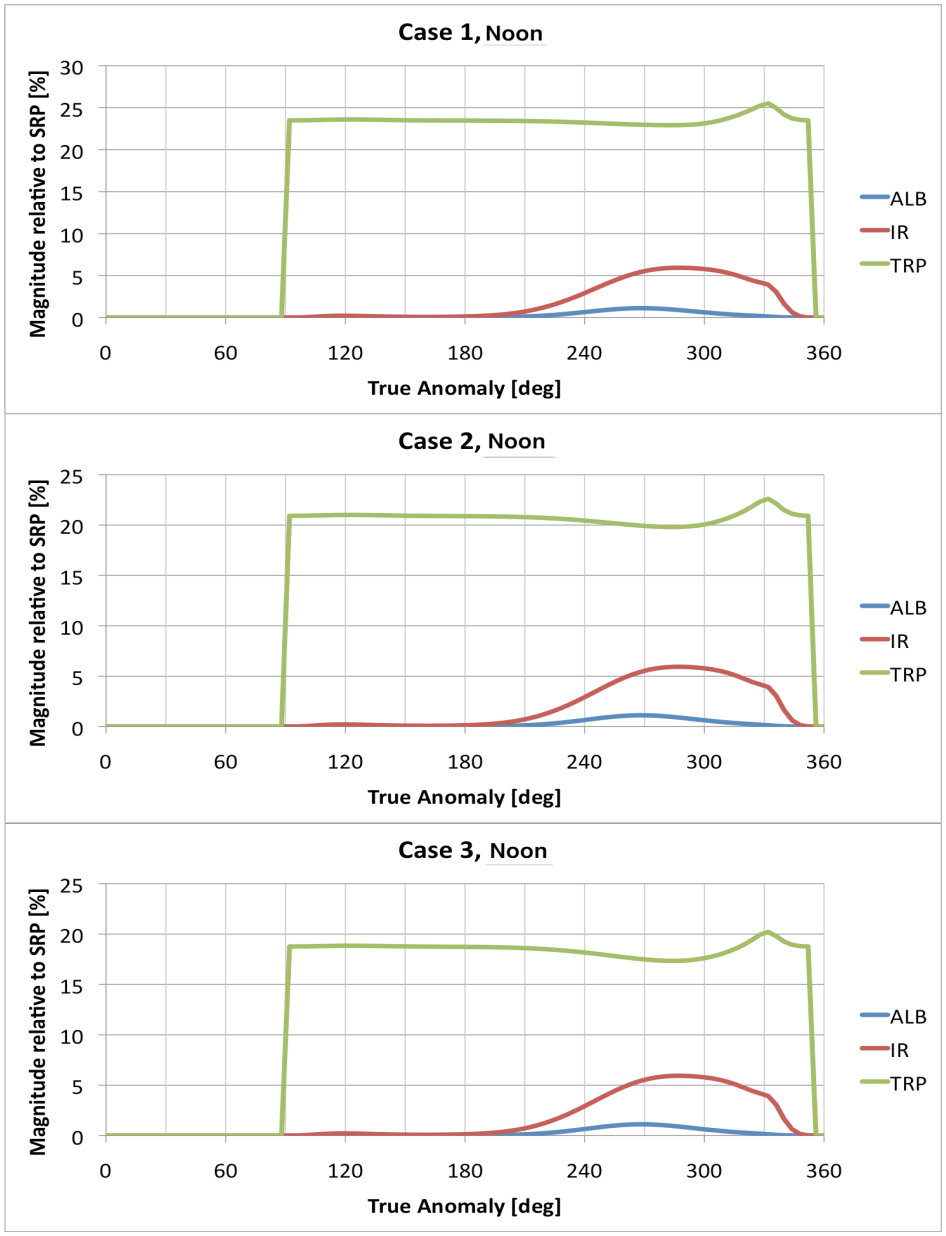

Figure 12. Percentages of Non-Gravitational Perturbations Relative to SRP for the 3 Cases for Noon orbits.

Table 5. SRP Magnitudes and Non-Gravitational Contributions Relative to SRP.

	SRP magnitude [m/s^2]	ALB [%]	IR [%]	TRP [%]
Case 1	8.49×10^{-7}	0.31	2.14	23.5
Case 2	5.84×10^{-7}	0.31	2.15	20.8
Case 3	3.69×10^{-7}	0.31	2.15	18.5

The ratio of the TRP effects gradually decreases for the three cases from about 24 to 19 % with the Mercury progression in its elliptical orbit around the Sun. On the other hand, the ratios of the ALB and IR contributions stay almost constant.

CONCLUSION

An analytical method for predicting the non-gravitational accelerations acting on a Mercury orbiter has been presented and demonstrated by using the MESSENGER mission and spacecraft parameters. The contributions of the Albedo reflection and planetary InfraRed radiation have been revealed by a straightforward approach. It is found that TRP effects dominate those induced by the InfraRed and Albedo radiations. The results show that the TRP effects are within the range from 19 to 24 % relative to the SRP effects in the cases considered here. Further improvements in the predictions may be expected by implementing more precise surface parameters for the spacecraft as well as for Mercury.

REFERENCES

[1] J. C. van der Ha and D. Stramaccioni, 'Thermal Radiation Effects on Deep-Space Trajectories', *Advances in the Astronautical Sciences - Spaceflight Mechanics 2010*, Vol. 136, 2010, pp. 1861-1880.

[2] T. Kato and J. C. van der Ha, "Precise Modelling of Solar and Thermal Accelerations on Rosetta," *Acta Astronautica*, Vol. 72, 2012, pp. 165 - 177.

[3] B. Rievers, T. Kato, J. C. van der Ha and C. Laemmerzahl, "Numerical Prediction of Satellite Surface Forces with Application to Rosetta," 22nd *AAS/AIAA Space Flight Mechanics Meeting*, Charleston, SC, January 29 – February 2, 2012, Paper AAS 12-180.

[4] T. Kato, B. Rievers, J. C. van der Ha and C. Laemmerzahl, "Detailed Analysis of Solar and Thermal Accelerations on Deep-Space Satellites," 22nd *AAS/AIAA Space Flight Mechanics Meeting*, Charleston, SC, January 29 – February 2, 2012, Paper AAS 12-219.

[5] J. C. van der Ha, "Model for Thermal Radiation Recoil Accelerations of Interplanetary Satellites," *Proceedings of 28th International Symposium on Space Technology and Science*, Ginowan, Japan, June 5-12, 2011, Paper ISTS-2011-d-55.

[6] D. P. Moessner and J. V. McAdams, "The MESSENGER Spacecraft's Orbit-Phase Trajectory," *AAS/AIAA Astrodynamics Specialist Conference*, Girdwood, AK, July 31 – August 4, 2011, Paper AAS 11-547.

[7] D. R. Stanbridge, K. E. Williams, A. H. Taylor, B. R. Page, C. G. Bryan, D. W. Dunham, et al., "Achievable Force Model Accuracies for MESSENGER in Mercury Orbit," *AAS/AIAA Astrodynamics Specialist Conference*, Girdwood, AK, July 31 – August 4, 2011, Paper AAS 11-548.

[8] C. J. Scott, J. V. McAdams, D. P. Moessner, and C. Ercol, "Modeling The Effects of Albedo and Infrared Radiation Pressures on The MESSENGER Spacecraft," *AAS/AIAA Astrodynamics Specialist Conference*, Girdwood, AK, July 31 – August 4, 2011, Paper AAS 11-552.

[9] Y. Sugimoto, J. C. van der Ha and B. Rievers, "Thermal Radiation Model for Rosetta Spacecraft," *AIAA Guidance, Navigation, and Control Conference*, Toronto, Canada, August 2-5, 2010, Paper AIAA-2010-7659.

[10] D. R. Williams, "Mercury Fact Sheet," NASA, http://nssdc.gsfc.nasa.gov/planetary/factsheet/mercuryfact.html.

[11] D. Garcia, R. Jehn, J. Schoenmaekers and P. de Pascale, "BepiColombo Mercury Cornerstone Consolidated Report on Mission Analysis," ESOC, MAO Working Paper No. 466, BC-ESC-RP-05500, April 2010.

[12] R. E. Smith and G. S. West compilers, "Space and Planetary Environment Criteria Guidelines for Use in Space Vehicle Development, 1982 Revision," NASA Technical Memorandum 82478, 1983.

[13] F.P. Incropera, D. P. DeWitt, T. L. Bergman and A. S. Lavine, "Fundamentals of Heat and Mass Transfer, 6th edition," Wiley, March, 2006, Chapter 12, pp. 724 - 730.